Supporting Appendix

Bending of the Microtubule Tip and Progression of the Path

We calculate the average microtubule trajectory under a force density f_e directed along the x-axis (Fig. 5*a*). The microtubule's path coordinates s, θ are defined within the cartesian reference frame as depicted in the figure. As explained in the main text, the average curvature of the microtubule path $\langle d\theta/ds \rangle$ is related to the microscopic bending of the microtubule tip ${\theta'}_{\rm m}(s)$ (Fig. 5*b*) as

$$\left\langle \frac{d\theta}{ds}(s) \right\rangle \approx \left\langle \frac{{\theta'}_{\rm m}(s)}{d} \right\rangle. \tag{5}$$

To determine the macroscopic $\theta(s)$ we need to calculate the microscopic bending ${\theta'}_{\rm m}(s)$ due to an external perpendicular force $f_\perp = f_{\rm e}\sin\theta(s)$.

Bending of the microtubule tip

We relate the microscopic bending of the microtubule tip to its material properties. We consider the bending of the free tip of length d (Fig. 5*c*) that is fixed in position and orientation ($\theta' = 0$) at the origin. Using the microscopic coordinates θ', s' as defined in the figure, we express the microscopic tip curvature as a function of the bending momentum $M(s')$ [1]

$$\frac{d\theta'}{ds'} = -\frac{M(s')}{EI}. \tag{6}$$

Here E is the bending modulus and I is the second moment of inertia. We calculate the internal shear force $F(s')$ and internal bending momentum $M(s')$ on a cross section of the tip segment of length $(\langle d \rangle - s')$ (Fig. 5*d*). From force balance we find $F(s') = f_\perp(d - s')$ and from balance of momentum we find $M(s') = -\frac{f_\perp}{2}(d - s')^2$. Substituting $M(s')$ into Eq. **6** we obtain an expression for the shape of the bent tip,

$$\frac{d\theta'}{ds'} = \frac{f_\perp}{2EI}(d - s')^2. \tag{7}$$

Solving this equation with the boundary condition $\theta'(0) = 0$ yields for the shape of the tip

$$\theta'(s') = \frac{f_\perp}{6EI}(s'^3 - 3ds'^2 + 3d^2 s'), \tag{8}$$

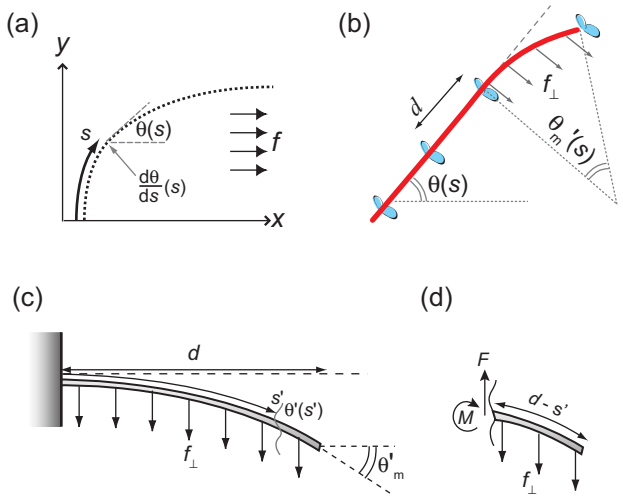

FIG. 5: (a) Microtubule trajectory under force density f along the x-axis. The path coordinates θ, s describe the trajectory. (b) The macroscopic path trajectory is described in terms of the microscopic bending of the microtubule tip θ'_{m} under the perpendicular force $f_{\perp}$, the magnitude of which is depending on the microtubule's orientation $\theta(s)$. (c) Bending of the tip in microscopic coordinates θ', s'. (d) Free-body-diagram of the microtubule tip defining the internal shear force F and bending momentum M as a function of position s'.

which defines the deviation at the end of the tip as $\theta'_{\mathrm{m}} = \frac{f_{\perp} d^3}{6EI}$. Substituting this in Eq. **5** we find that the local curvature of the microtubule trajectory is

$$\left\langle \frac{d\theta}{ds} \right\rangle = \left\langle \frac{f_e d^2}{6EI} \sin\theta \right\rangle . \tag{9}$$

For the averaging of the right-hand side of this equation, we use make use of the fact that the tip lengths d are exponentially distributed as a result of the random placement of kinesin motors on a a surface. The second moment $\langle d^2 \rangle$ of an exponential distribution with mean $\langle d \rangle$ equals $2\langle d \rangle^2$. This result, combined with the substitution of $EI{=}k_{\mathrm{b}}Tp$ yields

$$\left\langle \frac{d\theta}{ds} \right\rangle = \frac{f_e \langle d \rangle^2}{3k_{\mathrm{b}}Tp} \sin\theta. \tag{10}$$

.

Expression for the microtubule trajectory

Having obtained an expression for the local curvature (Eq. **9**), we now find the expression for the microtubule trajectory. For this purpose, we will express the path curvature in cartesian coordinates as

$$\frac{d\theta}{ds} = \frac{1}{[1+(\frac{dy}{dx})^2]^{3/2}}\frac{d^2y}{dx^2}. \tag{11}$$

To circumvent an infinite boundary condition at the origin ($\frac{dy}{dx} \equiv \infty$) we will solve the trajectory for a microtubule starting at the origin oriented along the x-axis, and subjected to a force density directed along the y-axis. In the final solution we will then interchange the x and y coordinates to arrive at a description for the trajectory as depicted in Fig. 5*a*. Thus, we combine Eqs. **9-11** where we replace $\sin\theta$ with $\cos\theta$ because of the axis interchange. Rewriting $\cos(\theta) = [1+(\frac{dy}{dx})^2]^{-1/2}$ we arrive at the differential equation describing the microtubule trajectory

$$\frac{d^2y}{dx^2} = [1+(\frac{dy}{dx})^2]\frac{f_e\langle d\rangle^2}{3k_bTp}. \tag{12}$$

Solving the equation with initial conditions $\frac{dy}{dx}|_0 = 0$, and $y(0) = 0$ we find that $y(x) = -R_0\ln(\cos\frac{x}{R_0})$, where $R_0 = \frac{3k_bTp}{f_e\langle d\rangle^2}$. Interchanging the x and y coordinates according to Fig. 5*a* we obtain

$$y(x) = R_0\arccos(e^{-\frac{x}{R_0}}). \tag{13}$$

Magnitude of the Electric Field-Induced Force

We calculate the expression for the electric field-induced force in the situation of stationary electrophoresis, that is, the force that is exerted on a charged object which is prevented from moving in an electric field. We show a cartoon of the experimental situation Fig. 6*a*. A negatively charged microtubule is subjected to an electric field $E_\perp$ which is directed perpendicular to its long axis. The field exerts a force per unit length of the microtubule which we denote f_q. Moreover, the electric field also exerts force on the counter ions immediately around the microtubule. As a result of this, and additionally because of any electro-osmotic flow, the fluid will move around the microtubule and exert a force per unit length of the microtubule, f_{fluid}, in the direction indicated. Thus, the effect of the electric field is to exert

a net perpendicular force on the microtubule,

$$f_{\perp} = f_q + f_{\text{fluid}}, \tag{14}$$

which is balanced by the mechanical force f_{mech}, that is exerted through the kinesin molecules.

It remains to calculate the magnitude of the forces in Eq. **14**. The magnitude of the electrical force f_q equals $\lambda E_{\perp}$, where λ is the line-charge density of the microtubule. The magnitude of the fluid forces can be calculated from the fluid velocity profile $\mathbf{v}$ around the microtubule tip. This profile can be obtained from solving the Navier-Stokes equation,

$$\eta \nabla^2 \mathbf{v} + \nabla P = -\rho \nabla \psi. \tag{15}$$

The first term represents the viscous forces, with η the viscosity of the fluid, the second term represents the pressure forces, with P the hydrostatic pressure, and the last term denotes the electrical forces on the fluid, through the charge density ρ and potential ψ. In the situation of stationary electrophoresis, we need to solve Eq. **15** with the boundary conditions $\mathbf{v} = 0$ at positions 0 (microtubule surface) and X, where X denotes the surfaces of the channel walls (no-slip boundary condition). A schematic of the fluid velocity profile is depicted in Fig. 6*b*.

The linearity of the Navier-Stokes equations allows us to state the solution to Eq. **15** as $\mathbf{v}$=$\mathbf{v}_h + \mathbf{v}_e$ [2], where $\mathbf{v}_h$ is the solution to the homogeneous differential equation, and $\mathbf{v}_e$ is a particular solution to Eq. **15**. The boundary conditions request that $\mathbf{v}_h = \mathbf{v}_e = 0$ at the no-slip surfaces X and that $\mathbf{v}_h = -\mathbf{v}_e$ at the surface of the microtubule (Fig. 6 *b*-*d*). In other words, the solution to the problem of stationary electrophoresis can be found from a superposition of solutions to the following homogeneous and particular differential equations for $\mathbf{v}_h$ and $\mathbf{v}_e$, respectively (with $P_h + P_e = P$),

$$\begin{aligned} &\eta \nabla^2 \mathbf{v}_h + \nabla P_h = 0 \qquad &&\text{with } \mathbf{v}_h(X) = 0,\ \mathbf{v}_h(0) = -\mathbf{v}_e(0), \\ &\eta \nabla^2 \mathbf{v}_e + \nabla P_e = -\rho \nabla \psi \quad &&\text{with } \mathbf{v}_e(X) = 0,\ \mathbf{v}_e(0) = \mu_{\perp} E_{\perp}. \end{aligned} \tag{16}$$

These differential equations describe the well-known situations of (*i*) the motion of an object with a certain velocity $\mathbf{v}_h(0)$ by a non-electric force (Fig. 6*c*), that is, purely hydrodynamic motion, and (*ii*) the free electrophoresis of an object (Fig. 6*d*) with velocity $\mathbf{v}_e(0)$, due to its mobility $\mu_{\perp}$. For both situations the magnitude of the resultant fluid forces are

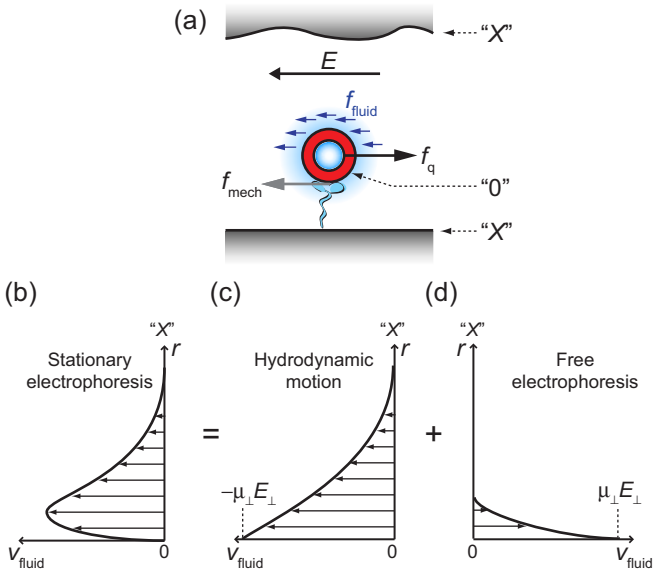

FIG. 6: (a) Schematic of the experimental situation. A microtubule is subjected to a perpendicular electric field $E_\perp$. The electric field exerts a force density $f_{\rm q}$ on the negatively charged microtubule. The moving fluid exerts a force density $f_{\rm fluid}$ which we calculate. The microtubule is hold taut by a mechanical force exerted by the kinesin $f_{\rm mech}$. (b-d) To calculate $f_{\rm fluid}$ we make use of the linearity of the Navier-Stokes equations. The schematic fluid velocity profile around the microtubule in stationary electrophoresis is shown in (b) as function of distance from the microtubule surface. This profile is a superposition of the fluid velocity profiles shown in (c-d). (c) Fluid velocity around an object that moves in purely hydrodynamic motion to the left with a velocity $-\mu_\perp E_\perp$. (d) Fluid velocity profile around an object in free electrophoresis, that moves to the right with a velocity $\mu_\perp E_\perp$.

known. In the case of purely hydrodynamic motion of an object with velocity $\mathbf{v}_h(0)$, the fluid forces have to balance the external force, and add up to $f_{\rm fluid,h} = -c_\perp \mathbf{v}_h(0)$, where $c_\perp$ is the Stokes-friction coefficient for the object. In the case of free electrophoresis, the fluid forces completely balance the electrical force on the object and thus $f_{\rm fluid,e} = -\lambda E_\perp$. Since $\mathbf{v}_h(0) = -\mu_\perp E_\perp$ (Fig. 6c, Eq. **16**), we calculate that $f_{\rm fluid,h} = c_\perp \mu_\perp E_\perp$. Therefore, in the case of stationary electrophoresis, the total force exerted by the fluid profile $\mathbf{v}$=$\mathbf{v}_h + \mathbf{v}_e$ around the stationary microtubule equals $c_\perp \mu_\perp E_\perp - \lambda E_\perp$. The total electric field-induced force (Eq. **14**) is thus equal to

$$f_\perp = c_\perp \mu_\perp E_\perp. \tag{17}$$

Measurement of the Perpendicular Mobility $\mu_{\perp,\mathrm{e}}$

We measure the value of $\mu_{\perp,\mathrm{e}}$ in Eq. **3** by performing electrophoresis experiments on freely suspended microtubules in channels as described previously [3]. In short, we coat the inside of straight 1 μm high channels with casein to prevent sticking of microtubules, with omission of kinesin, and then add microtubules. Upon application of an electric field, we observe the electrophoresis of individual microtubules in various orientations (Fig. 7). As expected, the electrophoretic motion of microtubules is in the direction opposite to the electric field. Because of their anisotropic mobility [3], microtubules that are oriented parallel to the electric field move faster than microtubules oriented perpendicular to the field (Fig. 7*a*). Fig. 7*b* is a plot of binned values of a large number ($\sim$5,800) of orientation-dependent velocities, measured with $E = 4\,\mathrm{kV/m}$. For the calibration of the perpendicular force (Eq. **3**) we are only interested in the velocity of microtubules oriented perpendicular to the electric field, $v_\perp = \mu_{\perp,e}E$. The inset in Fig. 7*b* shows measured values of $v_\perp$ for different electric fields. From the linear relation between $v_\perp$ and E we determine $\mu_{\perp,e} = -(1.03 \pm 0.01) \cdot 10^{-8}$ $\mathrm{m^2/Vs}$. We note that this value represents both the electrical properties of the microtubules as well as the electro-osmotic flow (EOF) velocity in the channel. We confirmed in separate experiments [3] that the additional coating of kinesin molecules had no significant influence on the EOF.

Measurement of the Bulk Persistence Length

We measure the value of the persistence length of long microtubules from the thermal fluctuations in their shapes. For this we follow the procedures and mathematical treatment as originally outlined by Gittes *et al.* [4]. In short, from a large number of shape fluctuations of an individual long microtubule that is suspended in a shallow experimental chamber, we determine the variance of the mode amplitudes of the shape-constituting fourier modes. The variance of these modes is a measure of the persistence length of the filament. We find that the bulk persistence length of our taxol-stabilized microtubules is 3.6 ± 0.3 mm (mean $\pm$ standard error) as measured from the first three modi of 7 different microtubules with contour lengths ranging from $22 - 41$ μm.

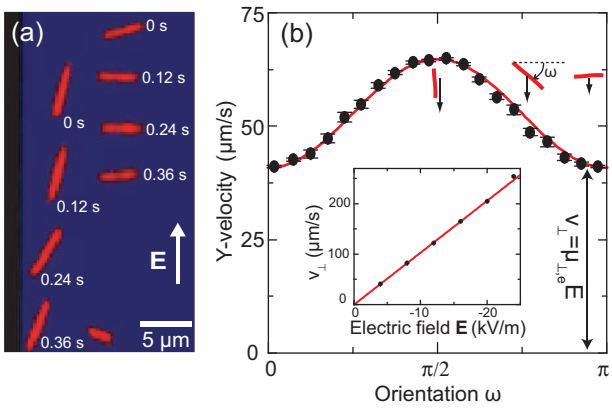

FIG. 7: (a) Overlay of snapshots with 0.12 s intervals of freely suspended microtubules in free electrophoresis ($E = 4$ kV/m). The velocity is orientation dependent as is obvious from these two microtubules in extreme orientations. (b) Binned data (5,800 data points) of orientation-dependent velocities under the same electric field. The inset shows the value of $v_\perp$ for different electric fields.

Materials and methods

Rhodamine-labeled microtubules were polymerized at 37 °C for 45 min at a concentration of 2 mg/ml in presence of 4 mM $MgCl_2$, 1 mM GTP and 5% DMSO in BRB80 buffer, and stabilized and 100× diluted in BRB80 containing 100 μM paclitaxel. Cover slips were cleaned by sonication in acetone, sulfuric acid, and ammonium-fluorid etchant, followed by a oxygen plasma treatment. Less than 1 μl of a microtubule containing solution in BRB80, supplemented with 100 μM Taxol, 120 mM D-glucose, 0.12 mg/ml glucose-oxidase, added on top, creating an experimental chamber with a thickness of approximately $1-3$ μm. The edges of the chamber were sealed with nail polish.

Fluorescence images of freely suspended microtubules were taken with a camera integration time of 20 ms and a time resolution of 1 s. The one-second interval between frames is long enough to prevent any serial correlation between the modes of microtubules, which can be estimated as maximum ∼1 s for the lowest mode of our longest microtubule (to calculate the mode relaxation time we refer to Eq. 32 in Ref. [4]). The integration time of 20 ms is sufficiently short to measure up to the first three modes of our longest microtubule, and up to the first two modes of our shortest microtubule (we estimate a 3-ms relaxation time for the third mode of a 22 μm long microtubule).

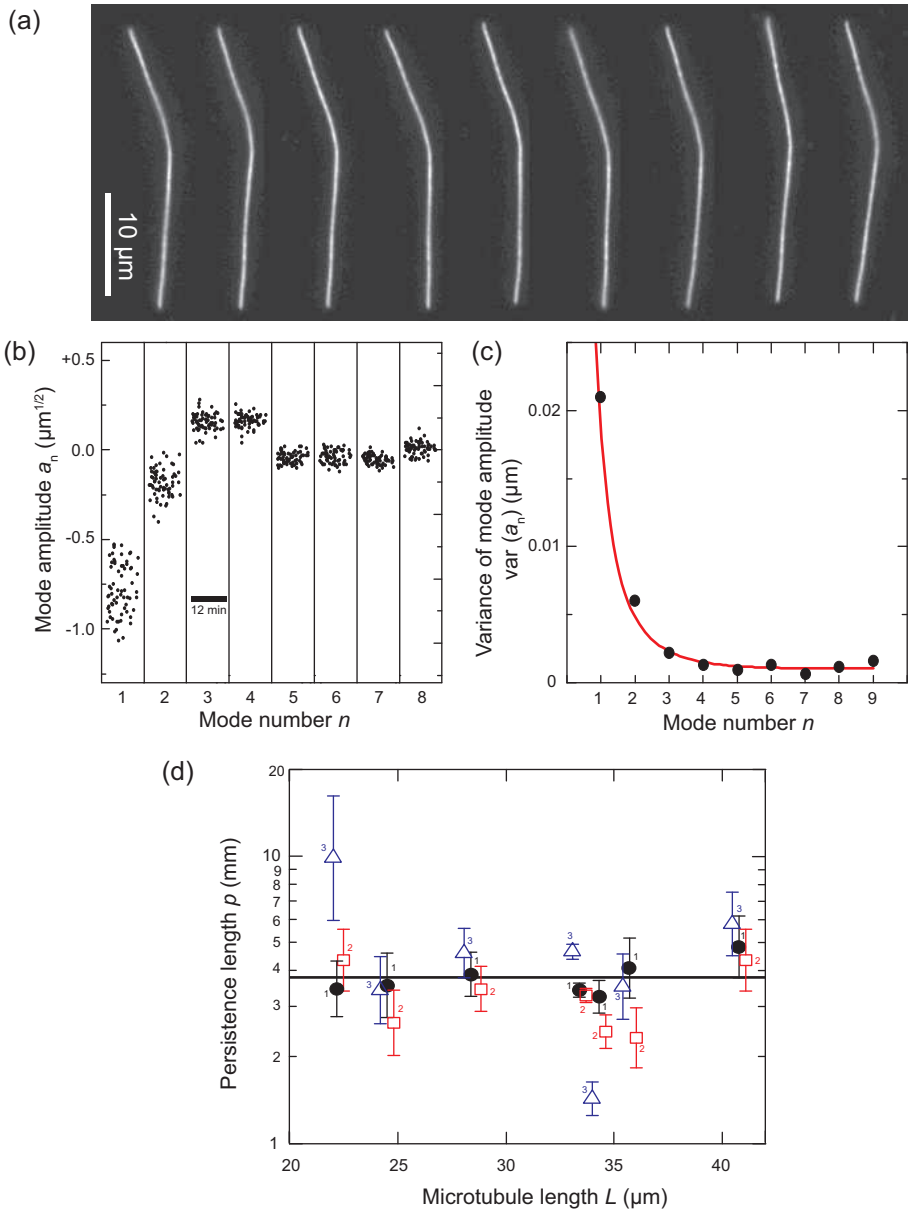

FIG. 8: (a) Snapshots of a 28 μm long microtubule. The time between the first and last snapshot is 70 seconds. (b) Mode amplitudes of the microtubule shown in a as a function of time. The non-zero averages of the different modes corresponds to the fixed curvature of the filament. (c) Variance of the mode amplitudes shown in b as a function of mode number. Red line is a fit of Eq. **18** according to the model presented in Eq. 17 in ref. [4]. (d) Persistence lengths obtained from different modes from 7 different microtubules. The values obtained from different modes of the same microtubule are slightly displaced along the x-axis for clarity, and the mode numbers are indicated. Error bars and the weighted average are calculated on the natural logarithm of the data as outlined in ref. [4]. The solid black line is the weighted average of all data points, with the exception of the two values for mode 3 at $L = 22$ and $L = 34$ μm.

Results

Fig. 8 shows, as an example, snapshots of a 28 μm long microtubule taken over a time period of 70 s. The microtubule has a distinct fixed curvature in addition to much smaller thermal fluctuations in its curvature. As described previously [4], we digitize 11 points along the microtubule contour length and calculate the tangent angles of the 10 segments between these points. The resulting tangent angle as a function of contour length was decomposed into nine different fourier cosine modes with mode amplitudes a_{n}, with $n = 1, \ldots, 9$.

Fig. 8*b* shows the mode amplitudes for the first eight modes as a function of time for this particular microtubule. The total observation time was 12 min and during this time the mode amplitudes show a distinct scatter around an average value which for the first two modes is smaller than zero due to the fixed curvature of the microtubule. The variance of the mode amplitudes is related to the persistence length of the filament.

In Fig. 8*c* we show the variance as a function of mode number. The variance contains contributions from the thermal fluctuations and from random measurement errors in the position of the microtubule. The red line in the figure is a fit of a model that captures both the thermal fluctuations as well as the random digitization errors (Eq. 17 in ref. [4]):

$$\mathrm{var}\left(a_{\mathrm{n}}\right) = \left(\frac{L}{n\pi}\right)^2 \frac{1}{p} + \frac{4}{L}\left\langle \varepsilon_{\mathrm{k}}^2 \right\rangle \left[1 + (N-1)\sin^2\left(\frac{n\pi}{2N}\right)\right]. \tag{18}$$

Here, N is the number of segments in the microtubule, and $\langle \varepsilon_{\mathrm{k}}^2 \rangle$ is the random error distance by which the microtubule positions are digitized. In this equation, the first term represent the variance introduced by thermal fluctuations and the second term represent the variance due to the digitization errors, $\langle \mathrm{a}_n^2 \rangle^{\mathrm{noise}}$. From the fit (with fit parameters p and $\langle \varepsilon_{\mathrm{k}}^2 \rangle$) we determine the magnitude of this experimental error to the measured variance, which can be subtracted from the measured variance to find the variance induced due to thermal fluctuations at each mode number, which yields a value for the persistence length for each mode:

$$\frac{1}{p} = \left(\frac{n\pi}{L}\right)^2 \left[\mathrm{var}\left(a_{\mathrm{n}}\right)^{\mathrm{measured}} - \left\langle \mathrm{a}_n^2 \right\rangle^{\mathrm{noise}}\right] \tag{19}$$

For the particular microtubule shown in the figure, we calculate the persistence length from the first three modes using Eq. **19** (Eq. 18 in ref. [4]). The natural logarithms of the persistence length from the three modes of this 28 μm long microtubule are plotted in Fig. 8*d*, together with the values obtained from six other microtubules. The persistence

lengths obtained from the different modes and from different microtubules are consistent, with the exception of the values obtained from the third modes of the microtubules with lengths of 22 and 34 μm. Excluding the latter two data points, the weighted mean and standard error of the persistence length is 3.6 ± 0.3 mm.

The high value of the persistence length for these long microtubules is in good agreement with other reports [4, 5], although our value is slightly lower. Note that the value that we find in this measurement represents a lower bound on the persistence length because we see in our images that microtubules have some freedom to rotate partially around their long axis. This rotation can contribute an additional variance to the measured mode amplitude, in particular when the microtubule has some fixed mean curvature.

[1] Landau, L & Lifshitz, E. (1986) *Theory of Elasticity, 3rd edition*, Course of Theoretical Physics, Volume 7. (Elsevier, Oxford, UK).

[2] Stigter, D & Bustamante, C. (1998) Theory for the hydrodynamic and electrophoretic stretch of tethered b-dna *Biophys. J.* **75**, 1197–1210.

[3] Van den Heuvel, M. G. L, De Graaff, M. P, & Dekker, C. (2007) Electrophoresis of individual microtubules in microchannels *Proc. Natl. Acad. Sci. U.S.A* **104**, 7770–7775.

[4] Gittes, F, Mickey, B, Nettleton, J, & Howard, J. (1993) Flexural rigidity of microtubules and actin-filaments measured from thermal fluctuations in shape *J. Cell Biol.* **120**, 923–934.

[5] Pampaloni, F, Lattanzi, G, Jonas, A, Surrey, T, Frey, E, & Florin, E. L. (2006) Thermal fluctuations of grafted microtubules provide evidence of a length-dependent persistence length *Proc. Natl. Acad. Sci. U.S.A* **103**, 10248–10253.